The cold gas content of bulgeless dwarf galaxies

Author(s):
Pilkington, K.; Gibson, B. K.; Calura, F.; Brooks, A. M.; Mayer, L.; Brook, C. B.; Stinson, G. S.; Thacker, R. J.; Few, C. G.; Cunnama, D.; Wadsley, J.

Publication date:
2011-11

Permanent link:
https://doi.org/10.3929/ethz-b-000041989

Originally published in:
Monthly Notices of the Royal Astronomical Society 417(4), https://doi.org/10.1111/j.1365-2966.2011.19450.x

Monthly Notices
of the
ROYAL ASTRONOMICAL SOCIETY

Mon. Not. R. Astron. Soc. **417,** 2891–2898 (2011) doi:10.1111/j.1365-2966.2011.19450.x

The cold gas content of bulgeless dwarf galaxies

K. Pilkington,[1,2]★ B. K. Gibson,[1,2] F. Calura,[1] A. M. Brooks,[3] L. Mayer,[4,5]
C. B. Brook,[1] G. S. Stinson,[1] R. J. Thacker,[2] C. G. Few,[1] D. Cunnama[6] and J. Wadsley[7]

[1]*Jeremiah Horrocks Institute, University of Central Lancashire, Preston PR1 2HE*
[2]*Department of Astronomy & Physics, St Mary's University, Halifax, Nova Scotia B3H 3C3, Canada*
[3]*Theoretical Astrophysics, Caltech, 1200 E. California Blvd., Pasadena, CA 91125, USA*
[4]*Institut für Theoretische Physik, University of Zürich, 8057 Zürich, Switzerland*
[5]*Department of Physics, Institut für Astronomie, ETH Zürich, 8093 Zürich, Switzerland*
[6]*Physics Department, University of the Western Cape, 7535 Cape Town, South Africa*
[7]*Department of Physics & Astronomy, McMaster University, Hamilton, ON L8S 4M1, Canada*

Accepted 2011 July 14. Received 2011 June 15; in original form 2010 September 2

ABSTRACT

We present an analysis of the neutral hydrogen (H I) properties of a fully cosmological hydrodynamical dwarf galaxy, run with varying simulation parameters. As reported by Governato et al., the high-resolution, high star formation density threshold version of this galaxy is the first simulation to result in the successful reproduction of a (dwarf) spiral galaxy without any associated stellar bulge. We have set out to compare in detail the H I distribution and kinematics of this simulated bulgeless disc with what is observed in a sample of nearby dwarfs. To do so, we extracted the radial gas density profiles, velocity dispersion (e.g. velocity ellipsoid and turbulence) and the power spectrum of structure within the cold interstellar medium (ISM) from the simulations. The highest resolution dwarf, when using a high-density star formation threshold comparable to densities of giant molecular clouds, possesses bulk characteristics consistent with those observed in nature, though the cold gas is not as radially extended as that observed in nearby dwarfs, resulting in somewhat excessive surface densities. The lines-of-sight velocity dispersion radial profiles have values that are in good agreement with the observed dwarf galaxies, but due to the fact that only the streaming velocities of particles are tracked, a correction to include the thermal velocities can lead to profiles that are quite flat. The ISM power spectra of the simulations appear to possess more power on smaller spatial scales than that of the Small Magellanic Cloud. We conclude that unavoidable limitations remain due to the unresolved physics of star formation and feedback within parsec-scale molecular clouds.

Key words: galaxies: dwarf – galaxies: evolution – galaxies: formation.

1 INTRODUCTION

A traditional problem plaguing the simulation of disc galaxies (e.g. Thacker & Couchman 2001; Abadi et al. 2003; Sommer-Larsen et al. 2003; Governato et al. 2004, 2007; Robertson et al. 2004; Bailin et al. 2005; Okamoto et al. 2005; Sánchez-Blázquez et al. 2009; Stinson et al. 2010, and references therein), within a cosmological context, has been the inability to recover successfully the properties of a truly 'late-type' disc and, in particular, those with essentially no associated stellar bulge, similar to classical galaxies such as M33.

Recent work by Governato et al. (2010), though, has produced what appears to be exactly such a bulgeless dwarf, via the imposition of a higher density threshold for star formation (100 cm^{-3}, as opposed to 0.1 cm^{-3}, as adopted in the aforementioned earlier generations of simulations), and mass resolution that allows one to identify individual star-forming regions.[1] The primary dwarf in their analysis[2] (DG1) forms a shallow central dark matter profile and possesses a pure exponential stellar disc of radial scale $r_d \sim 1$ kpc,

★E-mail: kpilkington@uclan.ac.uk

[1] The higher star formation density threshold can only be applied because the high resolution of the simulation, coupled with heating from the UV background, ensures fragmentation does not occur at unresolved scales.
[2] In addition to the supplementary re-simulation of DG1 described in Section 2.

with a stellar bulge-to-disc ratio B/D ≈ 0.04 as determined from the *i*-band light profile.

In what follows, we extend this work and examine in detail the cold neutral hydrogen (H I) gas content of the simulated dwarf DG1 along with its low star formation threshold analogue, DG1LT, and an updated version of DG1 (called nDG1) which employs high-temperature metal-line cooling and enhanced supernova (SN) energy feedback to compensate for the additional cooling. Our goal is simple: to determine if their H I gas properties agree with recent observational data to an equally successful degree as the stellar component. Studies such as the The H I Nearby Galaxy Survey (THINGS; Walter et al. 2008) provide excellent high-resolution (spectral and spatial) data against which to compare our simulations. The gas properties of the simulations are compared directly with several of the most recent relevant empirical data sets (Stanimirovic et al. 1999; Tamburro et al. 2009; O'Brien, Freeman & van der Kruit 2010), in order to assess both their strengths and weaknesses.

The cold gas in galaxies is linked directly to underlying star formation processes and associatedISM physics; any successful model of galaxy formation should adopt a holistic approach, examining both the gas and star properties in consort. We describe the basic properties of our simulations, before detailing the analyses undertaken; we will present results pertaining to the radial distribution of cold gas within the discs associated with DG1, DG1LT and nDG1, spatially resolved velocity dispersion maps of the cold gas, and the spatial distribution of power encoded within the structure of the ISM. We end with a summary of our findings, discussing both the strengths and weaknesses of the current simulations.

2 METHOD

2.1 Simulations

We have made use of the recent Governato et al. (2010) simulations which produced, for the first time, a late-type dwarf spiral with no associated stellar bulge. A full description of the simulations' characteristics is provided by Governato et al. (2010), but for context, it is useful to summarize their primary traits.

Using the *N*-body+smoothed particle hydrodynamics (SPH) (Monaghan 1992) code GASOLINE, a low-resolution (25 Mpc box, sufficient to provide realistic torques for these dwarfs), dark matter only simulation was used to identify $3.5 \times 10^{10}\,\mathrm{M}_\odot$ (virial) haloes (with typical spin paramters $\lambda = 0.05$) for potential (high-resolution) re-simulation using a volume renormalization technique (i.e.'zoom' simulation). New initial conditions were then re-constructed for the primary target halo (called 'DG1'), using the relevant low-frequency waves associated with tidal torquing in the low-resolution 'parent' simulation, but now enhanced with higher spatial frequencies generated after tracing the present-day particles back to the relevant Lagrangian subregion within the parent. The mass distribution was then sampled at higher resolution in the regions of interest, and more coarsely, further away from the identified halo. Both DG1 and nDG1 have a force resolution of 86 pc, while that of DG1LT is somewhat lower (116 pc); the initial baryonic (dark) particle mass for DG1 and nDG1 is $3300\,\mathrm{M}_\odot$ ($16\,000\,\mathrm{M}_\odot$), while for DG1LT it is $7800\,\mathrm{M}_\odot$ ($37\,000\,\mathrm{M}_\odot$). At $z = 0$, the *i*-band luminosities of DG1, nDG1 and DG1LT are $M_i = -16.5$, -15.8 and -19.1, respectively.

We should re-iterate that each of the three simulations described here (DG1, DG1LT and nDG1) use the same dark matter halo/assembly history, and differ primarily only in their treatment of the baryonic physics associated with star formation – i.e. either SN energy feedback efficiency (DG1 versus nDG1) or star formation density threshold resolution (DG1 versus DG1LT). DG1 was simulated using a star formation density threshold of $100\,\mathrm{cm}^{-3}$, typical of the densities encountered in giant molecular clouds, rather than the canonical value adopted in earlier simulations ($0.1\,\mathrm{cm}^{-3}$).[3] Other than the increased density threshold, two additional parametrizations were adopted, within the context of the feedback formalism employed: the star formation efficiency ($\epsilon\mathrm{SF} = 0.1$) and the fraction of SN energy coupled to the ISM ($\epsilon\mathrm{SN} = 0.4$). The star formation and feedback are modelled as described in Stinson et al. (2009). Without any additional ad hoc adjustments, this high-density threshold led to bulgeless dwarf spirals (akin to the classic prototype, M33) with flat (non-centrally concentrated) rotation curves (again, for the first time). Alongside our analysis of the high-threshold DG1 simulation, we provide a parallel analysis of two other simulated dwarfs, DG1LT (the lower threshold analogue, which uses the aforementioned canonical $0.1\,\mathrm{cm}^{-3}$ threshold, and a star formation efficiency $\epsilon\mathrm{SF} = 0.05$, with the same initial conditions as that used for DG1), and an updated version of DG1 and nDG1 [again with the same initial conditions as DG1 and a high-density threshold of $100\,\mathrm{cm}^{-3}$, but now with high-temperature metal-line cooling, after Shen et al. (2010), and increased thermal energy coupling to the ISM ($\epsilon\mathrm{SN} = 1$)], in order to better assess the role played by star formation threshold and feedback in 'setting' the gas properties of the respective simulations.

To foreshadow the discussion which will follow, perhaps the most problematic aspect of the current analysis is the uncertain numerical 'leap of faith' that must be made in associating the typically 7000–8000 K SPH gas particles, regardless of their local density ($\sim$0.1–$100\,\mathrm{cm}^{-3}$), with star formation (which in nature occurs in clouds and cores with temperatures 2–3 orders of magnitude lower than this). Until the effects of cooling by molecular hydrogen are incorporated fully within GASOLINE, this remains an unavoidable limitation of our modelling, but fortunately one whose effects are known and well understood. We return to this point in Sections 2.2 and 3.3.

2.2 Analysis

The cold gas properties of DG1, DG1LT and nDG1 are compared directly with those from comparable dwarfs in (Tamburro et al. 2009), in addition to the samples of O'Brien et al. (2010) and Stanimirovic et al. (1999). The bulk properties of DG1 (e.g. mass, luminosity and gas fraction) are consistent with those observed in nature (e.g. van den Bosch 2001; Walter et al. 2008), and its present-day star formation rate (SFR) ($\sim 0.005\,\mathrm{M}_\odot\,\mathrm{yr}^{-1}$) and luminosity ($M_i \approx -16$) are (specifically and directly) comparable to those of the three dwarfs from Tamburro et al. (2009), with Holmberg II (Ho II) being perhaps the closest direct analogue (and, as such, being the empirical counterpart to which we will refer DG1 most often). As noted earlier, the properties which we derive include the radial extent, the velocity dispersion as a function of galactocentric radius and the power spectrum of the ISM.

In our work, unless otherwise stated, we label 'cold gas' those SPH particles with temperatures less than $T_{\max} = 15\,000$ K [after Stinson et al. (2006)]. The bulk of the gas in DG1 (nDG1) lies near 7000 K (9000 K), which at face value would appear to be more appropriate for the warm H I phase of the ISM, rather than the

[3] GASOLINE employs an ideal gas law equation of state (Wadsley, Stadel & Quinn 2004), and the mean molecular weight is implicitly solved for and allowed to vary (Shen, Wadsley & Stinson 2010).

cold, star-forming, gas, to which we have associated star formation within the simulation. However, our cooling, despite the inclusion of metal-line cooling, is limited primarily to hydrogen and helium cooling, which can only cool gas down to these temperatures, and as emphasized in Stinson et al (2006; Section 5.1.1), we are averaging over scales much larger than individual star-forming cores. The effect of varying this maximum temperature threshold ($T_{\rm max}$) for star formation was examined in detail by Stinson et al. (2006) to which the reader is referred. We can summarize that analysis by stating that provided $T_{\rm max}$ is chosen to be not too similar in value to that of the mean temperature of the gas particles, its specific value does not critically affect star formation [see also, Shen et al. (2010)]. Efforts are underway to implement molecular hydrogen cooling within GASOLINE, after which a quantitative comparison with our results can be undertaken.

DG1LT, the low-density threshold analogue to DG1, is analysed in parallel to provide something of a canonical 'control' sample. As described in Governato et al. (2010), the properties of DG1LT [e.g. rotation curve, dark matter density profile and bulge-to-disc (B/D) ratio] are not well matched to those observed in nature, due to the traditional limitations that the new suite of simulations were designed to overcome in the first place. As a juxtaposition to DG1 though, it is invaluable. The present day SFR ($0.2\,{\rm M}_\odot\,{\rm yr}^{-1}$) and luminosity ($M_i = -19.1$) are much higher than that of DG1 (and the associated stellar mass is correspondingly a factor of ten higher), driven [as described by Governato et al. (2010)] by its adoption of the lower star formation threshold (see Fig. 1).

For our analysis, we have generated a new variant of DG1 (labelled nDG1), employing both the same initial conditions and higher star formation threshold ($100\,{\rm cm}^{-3}$). As alluded to earlier, where nDG1 differs from its predecessors is in its inclusion of metal-line cooling [following Shen et al. (2010)] and a more efficient coupling of SN thermal energy to the ISM; qualitatively, we can anticipate this leading to a somewhat more turbulent ISM. On the whole, the SFR of nDG1 is suppressed relative to DG1, but extends to lower redshifts (Fig. 1, where one can see that the SFR from $8 \lesssim t \lesssim 10\,{\rm Gyr}$ is $\sim 10\times$ higher in nDG1 than in DG1); its luminosity is, not surprisingly, somewhat lower than that of DG1 ($M_i = -15.8$, as opposed to $M_i = -16.5$), considering its stellar mass is a factor of 2 lower ($M_* \approx 2.1 \times 10^8\,{\rm M}_\odot$ versus $M_* \approx 4.4 \times 10^8\,{\rm M}_\odot$).

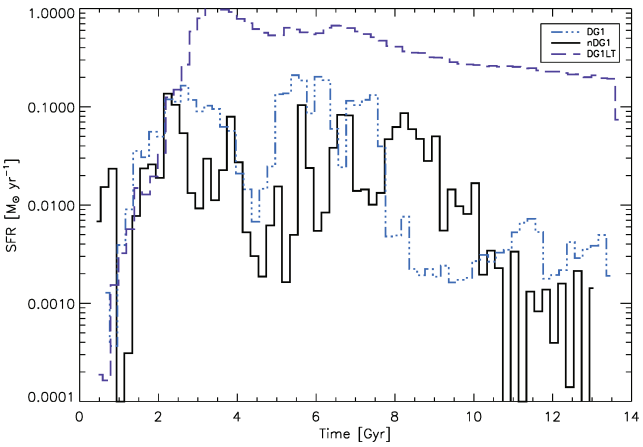

Figure 1. The SFRs of nDG1 (solid line), DG1 (dot–dashed line), and DG1LT (dashed line). Star formation in nDG1 is suppressed overall, relative to DG1, but extends $\sim$2 Gyr beyond the cessation of bulk star formation in DG1 (in the range $8 \lesssim t \lesssim 10$ Gyr). There is intermittent star formation in both dwarfs up to the present day, but it has been consistently low for the past $\sim$3 Gyr in nDG1 and $\sim$5 Gyr in DG1. The star formation history of DG1LT is overall considerably higher than its two higher density threshold analogues.

Zeroth (density), first (velocity) and second (velocity dispersion) moment maps of the simulated neutral hydrogen distributions were generated using TIPSY,[4] after matching the $\sim 40^\circ$ inclination of the dwarfs from the Tamburro et al. (2009) THINGS sample (which, again, includes Ho II, our primary analogue against which our simulations will be compared, as noted in Section 2). The conversion from 'cold gas' to 'H I' within GASOLINE suffices for the purposes outlined here; the values derived are close to the values one would predict under the assumption of combined photoionization and collisional ionization equilibrium. All our results were cross-checked using both cold gas and H I moment maps, in addition to further cross-checks undertaken after eliminating high column density H I gas for which the conversion from cold gas to H I is most insecure. The results described here are robust to these choices, and for expediency are not discussed further.

Our velocity dispersion analysis made use of the second H I moment map derived from the line-of-sight dispersion map produced from viewing the DG1, nDG1 and DG1LT simulations with an inclination angle matching that of Ho II. For the analysis of the distribution of structural 'power' within the cold ISM of the simulations, we again used the zeroth H I moment maps and their Fourier transforms and compared the inferred power-law spectra with that derived for the Small Magellanic Cloud (SMC) by Stanimirovic et al. (1999).

3 RESULTS

3.1 Radial density profiles

We first confirmed independently that the stellar light associated with DG1 was indeed consistent with a pure exponential of scalelength $\sim$1 kpc (i.e. bulgeless) disc [akin to the Type I profiles categorized by, for example, Pohlen & Trujillo (2006)]; as shown in the lower panel of Fig. 2, this was the case. DG1LT also has a radial (stellar) scalelength of $\sim$1 kpc, but shows the classical 'problem' of possessing a substantive stellar bulge within the inner kiloparsec (B/D ≈ 0.2). The stellar disc component of nDG1 is not well represented by a single pure exponential (cf. DG1); instead, its surface density profile shows a deficit of matter (and light) in the outskirts of the stellar disc (beyond a so-called break radius at $\sim$2–3 kpc), consistent with the more common Type II profiles observed in nature (e.g. Pohlen & Trujillo 2006; Sánchez-Blázquez et al. 2009); the inner and outer parts of the nDG1 stellar disc show radial scalelengths of $\sim$2 and $\sim$1 kpc, respectively. The B/D ratio of nDG1 matches formally that of DG1, although it is also readily apparent that the surface density (and light) profile of nDG1 shows a high-density stellar 'core', in which $\sim 10^7\,{\rm M}_\odot$ ($\sim$10 per cent of the nDG1 stellar mass, as a whole) is concentrated within the inner 100 pc. Importantly, this stellar 'core' is inconsistent with a bulge. Instead, it consists of a large cluster of stars that was formed in the disc during a merger at high redshift, and traveled inward with time so that at $z = 0$ it is close to, but not located at, the dynamical centre of the galaxy (i.e. it can be seen to rotate about the galaxy centre).

The cold gas of DG1 displays a rapid increase in density within $\sim$1 kpc. Exterior to this is an extended disc with an exponential scalelength $r_{\rm d} \sim 6$ kpc; the cold gas disc truncates at $\sim 1 r_{\rm d}$, somewhat short of those observed by Tamburro et al. (2009) and O'Brien

[4] www-hpcc.astro.washington.edu/tools/tipsy/tipsy.html

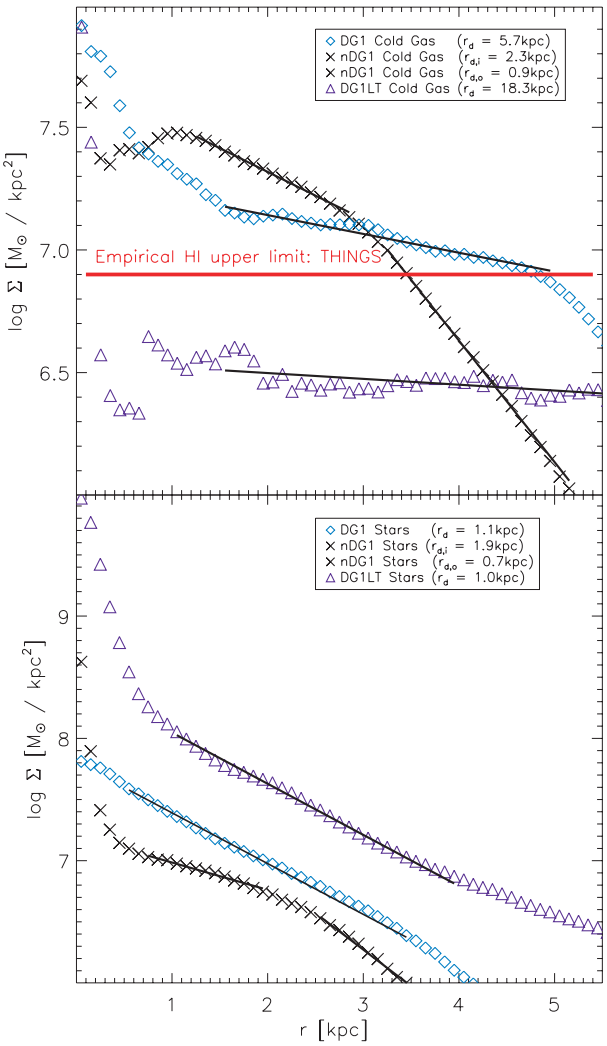

Figure 2. Radial gas (top) and stellar (bottom) density profiles for the simulated dwarfs DG1 (diamonds), DG1LT (triangles) and nDG1 (crosses). The thick overplotted lines show the exponential fits to the distributions, from which the noted scalelengths were derived. The stellar component of DG1 obeys a pure exponential of scalelength ∼1 kpc, with no evidence for a central bulge, while both nDG1 and DG1LT show central cores. Both the stellar and cold gas components of nDG1 are best represented by double exponentials, with a break between the two near ∼3 kpc. The cold gas of DG1 is distributed in a more extended exponential disc component of scalelength ∼6 kpc, while that of DG1LT is ∼18 kpc. The horizontal line in the upper panel corresponds to the empirical upper limit to H I encountered in nature, from the THINGS work (Bigiel et al. 2008).

et al. (2010), where the respective H I discs are traced out to ∼2–6r_d. Bigiel et al. (2008) showed that there is an empirical H I upper limit encountered in nature – $\Sigma_{HI} \lesssim 9\,M_\odot\,pc^{-2}$. This upper limit is represented by the horizontal line in the upper panel of Fig. 2. Because we do not yet resolve the microphysics associated with molecular processes on parsec-scales, one might ascribe some fraction of the cold gas in the simulation [particularly that above the upper limit observed by Bigiel et al. (2008)]. to molecular gas. Again using the results from Bigiel et al. for the fraction of H_2/H I as a function of radius (see their fig. 13), we can verify that the high-density gas interior to 1 kpc is consistent with being molecular gas. In particular, r_{25}, the isophotal radius corresponding to 25 mag arcsec^{-2}, is 2.0 kpc for DG1. Assuming that as much of the gas can be ascribed to H I as possible (i.e. the upper limit of $\Sigma_{HI} = 9\,M_\odot\,pc^{-2}$), then the results from Bigiel et al. suggest that $7.9\,M_\odot\,pc^{-2}$ would typically be in molecular gas at the innermost radius of DG1, dropping to $7.2\,M_\odot\,pc^{-2}$ at 0.8 kpc, and declining rapidly to $\lesssim$0.1 H_2/H I at 2 kpc. That is, while the total amount of gas in DG1 is consistent with empirical bulk scaling relations, and the gas within 1 kpc is consistent with being mostly molecular, the cold gas surface densities beyond 1 kpc are too high relative to nature.[5]

It is difficult to interpret the source of this excess gas. Perhaps this is the gas that should instead be lost from the galaxy in winds. While it may be tempting to suggest that this gas is overly concentrated, comparison of the cold gas scalelengths for these simulated galaxies (which has been fit beyond r_{25}) to the scalelengths beyond r_{25}, in the sample of Bigiel et al. (2010), suggests that the excess gas in these simulations is actually too extended compared to real galaxies. Alternatively, as discussed below for the case of DG1LT, additional star formation in the outskirts of the simulated galaxy discs could decrease the surface density of gas (as it goes instead into stars). While Brooks et al. (2011) showed that the *B*-band scalelength of DG1 is comparable to observed dwarf galaxies, a factor of 1.5–2 increase in size is still allowable to be fully consistent with nature. In fact, preliminary tests of molecular cooling and star formation in GASOLINE suggest that the star formation is more extended at $z = 0$. Hence, the addition of H_2 to these simulations may alleviate the problem of this excess gas.

As was the case for the stellar light, the disc of nDG1 is better represented by a 'broken', or two-component exponential, with inner and outer disc scalelengths of ∼2 and ∼1 kpc, respectively (with the break occurring near a galactocentric radius of ∼3 kpc). The arguments of the previous paragraph concerning the excess surface density of the cold gas in DG1 applies obviously to nDG1, as well.

Conversely, the cold gas in the disc of DG1LT extends radially to ∼8 kpc with an essentially flat density profile (formally, with a radial scalelength of ∼18 kpc – i.e. , the gas disc truncates near ∼0.5r_d – again, short of the typical disc in nature, but since the profile is so flat, the formal exponential 'scalelength' is somewhat ill defined). Like DG1, DG1LT also shows a high-density cold gas 'core' (of mass $\sim 2 \times 10^6\,M_\odot$), although it is somewhat more extreme, in the sense of it being concentrated solely within the inner ∼100 pc (note that this is within twice the force softening length). Being more extended, and the gas fraction being an order of magnitude lower [Governato et al. (2010), table 2], it is not surprising that the cold gas surface density profile of DG1LT is consistently a factor of ∼3× lower than the empirical upper limit derived by (Bigiel et al. 2008). However, this result should not be interpreted to mean that DG1LT is the more realistic version of this galaxy simulation. As Governato et al. (2010) and Oh et al. (2011) have demonstrated clearly, the mass of this galaxy is overly concentrated, with a large bulge and peaked inner rotation curve that are inconsistent with the observed galaxies in the same mass range.

3.2 Velocity dispersion

We next undertook an examination of the velocity dispersion of the H I discs of DG1, nDG1 and DG1LT, to make a comparison with those observed in various samples of dwarfs in the literature

[5] We note that while this is a sample of one, additional simulations from the same suite [e.g. DG2 from (Governato et al. 2010)] show the same behaviour; we have chosen to focus only upon DG1, for clarity.

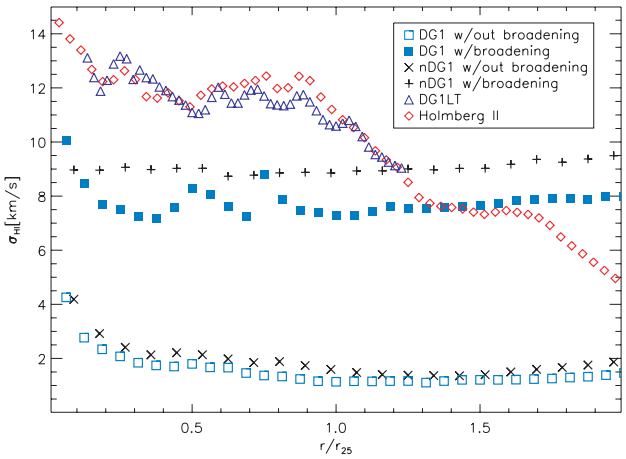

Figure 3. Radial behaviour (in units of the *B*-band r_{25} - i.e. the isophotal radius corresponding to 25 mag arcsec^{-2} or, roughly, to the extent of the star-forming disc) of the H I line-of-sight velocity dispersion of the DG1 (open squares), DG1LT (triangles) and nDG1 (crosses) simulations, derived from the SPH gas particles' 'streaming velocities' [after van den Bosch et al. (2002)], in addition to the true H I line-of-sight velocity dispersion profile for DG1 (filled squares) and nDG1 (plus signs), after correcting the streaming velocities isotropically for their internal thermal energies. Also shown is a representative dwarf spiral from the THINGS (Tamburro et al. 2009) sample (Ho II: diamonds). Note: r_{25} is 2.0 , 5.5, 1.4 and 3.3 kpc, respectively, for DG1, DG1LT, nDG1 and Ho II.

(Crosthwaite, Turner & Ho 2000; Crosthwaite et al. 2001; Tamburro et al. 2009; O'Brien, Freeman & van der Kruit 2010). Observations show that independent of present-day SFR, luminosity or mass, discs possess a characteristic velocity dispersion of ∼8–10 km s^{-1}, rising to ∼12–15 km s^{-1} in the inner star-forming regions (i.e. within r_{25}, the isophotal radius corresponding to 25 mag arcsec^{-2}).[6] A typical radial velocity dispersion distribution is shown in Fig. 3 for Ho II (plus signs), from the THINGS sample (Tamburro et al. 2009).

In addition to the curve for Ho II, in Fig. 3 we also show the corresponding velocity dispersion profiles (line of sight, assuming again a ∼40° inclination, similar to that of Ho II) for DG1 (open diamonds), nDG1 (crosses) and DG1LT (triangles), derived from the SPH gas particles' *streaming velocities*[see below, and van den Bosch et al. (2002)], and for DG1 (filled diamonds), taking into account said particles' *thermal velocities*. Circular annuli[7] projected on the inclined galaxy were used to set the bins.

For typical Milky-Way-scale simulations, the thermal broadening component is often neglected, since the 'streaming velocity' of the SPH particle usually dominates over the 'thermal component'. For our simulated dwarfs, this is clearly inadequate, as the streaming velocity dispersion can be much smaller than the relevant thermal velocity dispersion. To incorporate the latter, we follow the procedure outlined by van den Bosch et al. (2002) (Section 2.3) and note that the velocity of each particle can be written as $v = u + w$, where u is the mean streaming velocity at the location x and w is the particle's random (thermal) velocity. Because SPH only tracks the streaming motions of the particles, we make use of the internal energy of each particle, in order to derive an appropriate random component to apply to each particle. In practice, we draw random velocities for each Cartesian coordinate from a Gaussian of dispersion $\sigma = \sqrt{kT/\mu}$ and add those to each of the coordinates of the streaming motion, where T is the temperature of the gas particle (typically, ∼7000–9000 K, for our simulations), k is Boltzmann's constant, and μ is the mean molecular weight of the gas.

Without the inclusion of thermal broadening, both DG1 and nDG1 show extremely (and unphysically) kinematically cold ISM compared to DG1LT and, more importantly, dwarfs in nature [compare the crosses and open squares of Fig. 3 (simulations) with those of the plus symbols (observations) for a graphic example of the mismatch between unphysical streaming velocity dispersions and those encountered in nature]. This does not imply, however, that DG1LT as presented in Fig. 3 is physical. First, and most importantly, as already noted in Section 3.1 and, especially, by Governato et al. (2010) and Oh et al. (2011), the rotation curve and dynamics of DG1LT are problematic, as is the associated significant overproduction of the stellar bulge. As can be seen in Fig. 1, DG1LT has an SFR of two orders of magnitude larger than DG1 or nDG1; while this does not impact upon its consistency with the stellar mass–metallicity, luminosity–metallicity or H I gas fraction–luminosity scaling relations, it does worsen significantly the consistency with the dynamical-to-stellar mass ratio distribution of Blanton, Geha & West (2008). This large SFR drives more turbulence, leading to the large streaming velocities for this simulation. We have not included the thermal component for DG1LT in Fig. 3, as doing so would only increase its velocity dispersion from ∼12 to ∼14 km s^{-1}. The inferred line-of-sight velocity dispersion profile for DG1, after application of the above thermal broadening (which effectively amounts to a σ ∼ 7–9 km s^{-1} broadening of the essentially negligible ∼1 km s^{-1} streaming motions), is represented by the filled squares in Fig. 3.

The characteristic velocity dispersions of the cold gas within DG1 and nDG1 are comparable to those encountered in nature [∼8–10 km s^{-1}; Tamburro et al. (2009)] when thermal velocities are considered. The thermally broadened velocity dispersion profile of DG1 shows a few enhanced features (near $0.5r_{25}$). These are due to high-temperature gas particles in and around superbubbles blown by supernovae (SNe) feedback (discussed further below and shown in Fig. 4). By design, including a random thermal component to the velocity dispersion accentuates these features. However, by chance, the particular time-step we examine here for nDG1 does not show any bubbles (though does at previous time-steps), and hence no thermal features are introduced into the profile of this simulation. As can be seen from the streaming-only profiles for these galaxies, both have slightly higher macroscopic velocity dispersions in the inner few hundred parsecs. However, in DG1 this gas is ∼35 per cent hotter than the rest of the disc, while in nDG1 it is cooler by a similar factor. Fig. 3 shows that, when this is considered in the thermally broadened velocity dispersions, it has the effect of maintaining the higher velocity dispersion structure in the inner region of DG1, while 'washing out' the inner structure in nDG1. This result highlights a conundrum in terms of comparing the velocity dispersion profiles of these dwarf galaxy simulations to real dwarfs.

A more subtle effect of imposing the random thermal velocity perturbation to each particle's streaming motion is that the velocity ellipsoid of the cold gas becomes necessarily isotropic, disguising any anisotropies that might have been present in the streaming motions (i.e. young stars, and the cold gas from which they formed,

[6] At the resolutions at which we are working (∼100 pc), the velocity dispersions of the molecular and neutral gas are not dramatically different (Crosthwaite et al. 2000, 2001).

[7] Technically, elliptical annuli should be used, but our results are not sensitive to this choice, at these inclination angles; in addition, we re-measured the velocity dispersion profile on the raw THINGS data for Ho II using circular annuli, to ensure self-consistency with our analysis of the simulations.

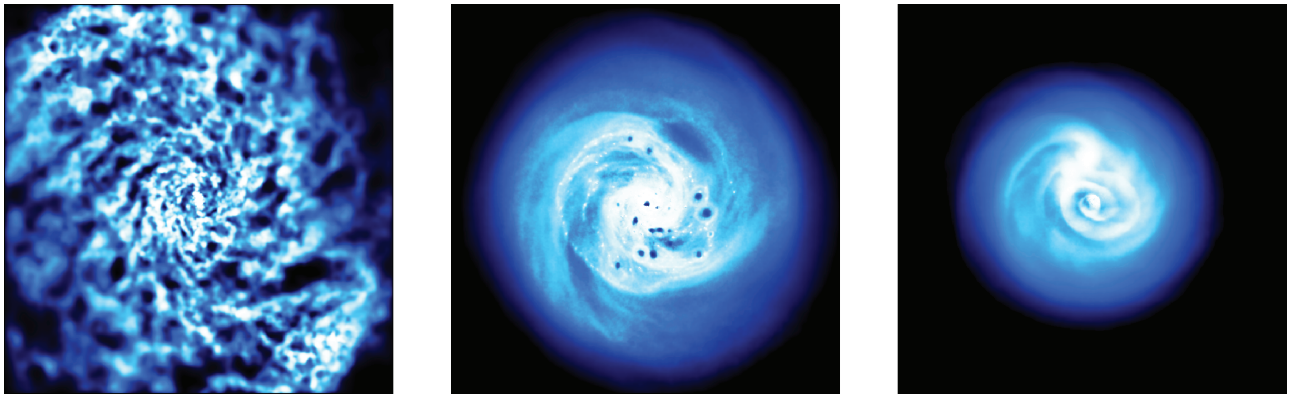

Figure 4. Neutral hydrogen (H I) moment zero maps of the three simulations analysed here - from left to right: DG1LT, DG1 and nDG1. Each panel has dimensions 14 × 14 kpc; a lower column density threshold of N(H I) $= 1 \times 10^{19}$ cm^{-2} was employed for each map.

will necessarily have different velocity ellipsoids). For example, for DG1 (nDG1), the radial, azimuthal and vertical velocity dispersions inferred from the cold gas particles' streaming motions, measured at $\sim 0.5 r_{\rm d}$, are $\sigma_r \approx 4\,{\rm km\,s^{-1}}$ ($\sim 6\,{\rm km\,s^{-1}}$), $\sigma_\phi \approx 3\,{\rm km\,s^{-1}}$ ($\sim 6\,{\rm km\,s^{-1}}$) and $\sigma_z \approx 1\,{\rm km\,s^{-1}}$ ($\sim 2\,{\rm km\,s^{-1}}$), i.e. σ_r:σ_ϕ:$\sigma_z \approx 3$:3:1 (anisotropic). After thermal broadening, the derived respective velocity dispersions are $\sigma_r \approx 8.5\,{\rm km\,s^{-1}}$ ($\sim 10\,{\rm km\,s^{-1}}$), $\sigma_\phi \approx 8\,{\rm km\,s^{-1}}$ ($\sim 10\,{\rm km\,s^{-1}}$) and $\sigma_z \approx 7.5\,{\rm km\,s^{-1}}$ ($\sim 8.5\,{\rm km\,s^{-1}}$), i.e. σ_r:σ_ϕ:$\sigma_z \approx$ 1:1:1 (isotropic). What this means is that an unavoidable outcome of our current inability to resolve parsec-scale molecular heating and cooling processes within the simulations is the lack of any significant correlation between velocity dispersion and galactocentric radius and/or underlying star formation. Until we can resolve densities (and temperatures) corresponding to the cores of molecular clouds, this apparent mismatch between observations and simulations would appear difficult to avoid.[8]

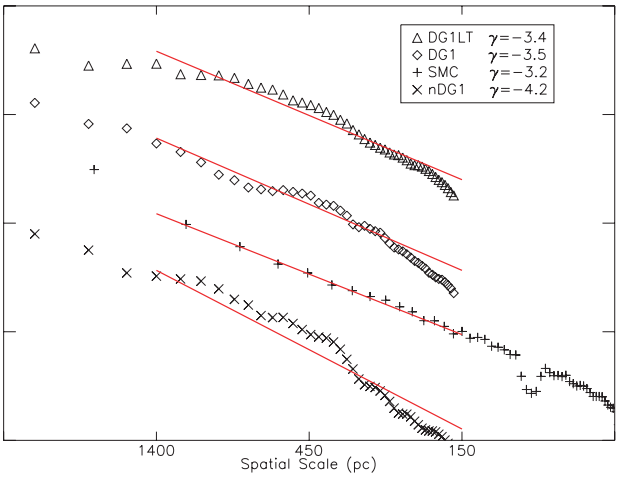

Figure 5. Spatial power spectra of the cold ISM of DG1 (diamonds), DG1LT (triangles), nDG1 (crosses) and the SMC (plus signs). Power-law slopes of −3.5, −3.4, −4.2 and −3.2 are overplotted for DG1, DG1LT, nDG1 and the SMC, respectively. The 'break' in the SMC power spectrum is due to a missing baseline in the Stanimirovic et al. (1999) Australian Telescope Compact Array (ATCA) data set. The power spectra for the three simulations have been truncated at ∼2 resolution elements (2×full width at half-maximum of the adopted Gaussian beam: ∼200 pc).

3.3 Power spectrum and superbubbles

Following Stanimirovic et al. (1999), we generated the Fourier transform of the H I moment zero maps of DG1, nDG1 and DG1LT – each shown in Fig. 4 at the same spatial scale (14 × 14 kpc) with the same limiting H I column density (N(H I) $> 1 \times 10^{19}$ cm^{-2}) – after first convolving the maps with a 100 pc Gaussian, to mimic the typical beam smearing present within THINGS data for Ho II (Tamburro et al. 2009). Circular annuli in Fourier space were then employed to derive the average power in the structure of the ISM on different spatial scales. Fig. 5 shows the derived power spectra for the simulations DG1, nDG1 and DG1LT, and that for the SMC, re-derived for self-consistency, using the H I data cube of Stanimirovic et al. (1999). Grossly speaking, the distributions can be represented by a power law of the form $P \propto k^{\gamma}$, with $\gamma = -3.5$ for DG1, $\gamma = -3.4$ for DG1LT, $\gamma = -4.2$ for nDG1 and $\gamma = -3.2$ for the SMC [consistent with that found originally by Stanimirovic et al. (1999), and consistent with the power spectrum expected when H I density fluctuations dominate the ISM structure, rather than turbulent velocity fluctuations, which dominate the spectrum when isolating 'thin' velocity slices].

There are several points to highlight from Fig. 5: (i) the SMC shows no evidence for departure from a pure power law, and hence there does not appear to be any obvious preferred H I cloud size in nature; (ii) broadly speaking, both DG1 and DG1LT are shallower than nDG1 (i.e. possess more power on smaller scales, rather than larger, relatively speaking); put another way, the enhanced feedback associated with nDG1 shifts power in the simulated ISM from smaller scales to larger scales, just as one might expect; (iii) each of the simulations shows a greater departure from a pure power law than does the SMC; the most obvious departure from a power law is perhaps seen in the enhanced power on ∼400–500 pc scales in nDG1. This enhanced power corresponds to the 'radial cadence', or frequency, of the tightly wound spiral structure in the inner few kiloparsecs of the simulation (apparent in the right-most panel of Fig. 4).

[8] It might be tempting to conclude that since the enhanced feedback did not result in a *significantly*higher line-of-sight velocity dispersion, this is consistent with the earlier work of Dib, Bell & Burkert (2006) and Petric & Rupen (2007), who concluded that SN feedback alone was insufficient to provide turbulent heating to the cold ISM in excess of a few km s^{-1}; in light of the fact that we are not resolving the ISM heating and cooling processes at parsec and subparsec scales, we feel it premature to draw such a conclusion from this aspect of our analysis.

Finally, from the present-day moment zero column density map of DG1 (middle panel of Fig. 4), we identified 13 SNe-driven superbubbles in its cold ISM. While we do not wish to belabour the point when employing such small-number statistics, it is re-assuring to note that upon plotting the superbubble size distribution, the data were consistent with a power-law slope between -1.5 and -2.0 (dependent upon normalization). Such slopes are entirely consistent with those observed in nearby dwarfs (Oey & Clarke 1997).

4 DISCUSSION

One immediate concern arising from our analysis relates to the issue of extracting 'neutral hydrogen' from the simulations' 'cold gas' (which in some sense consists of both molecular and neutral hydrogen). Because the high-density regions within the simulation have densities more akin to molecular, rather than neutral, clouds, it is important to explore the definition of 'neutral' employed here.[9] To do this, we re-generated H I moment maps, but now restricting the gas included to only those particles with densities near the classical value of $\sim 0.1\,\mathrm{cm}^{-3}$. As expected, this eliminated the unrealistically high neutral hydrogen column densities in the highest density regions, but at the expense of leading to vertical density profiles that bore little resemblance to the Gaussian profiles observed in nature (O'Brien et al. 2010). Such an extreme 'cut' to the definition of neutral hydrogen also led to a radial profile that bore little resemblance to an exponential. We found no density cut which impacted favourably on the observable properties of DG1. For these simulations, because density and temperature are closely correlated in the relevant regime ($T \lesssim 30\,000\,\mathrm{K}$; $\rho \gtrsim 0.001\,\mathrm{cm}^{-3}$), the above analysis is degenerate to cuts in volume density or temperature.

It is important to note that the primary process responsible for driving bulk properties in the simulation is the star formation and feedback prescription. Governato et al. (2010) demonstrated that star formation had a larger effect on the rotation curve of our simulated galaxy than resolution (see their fig. 5). The gas properties presented in this paper are primarily the result of the star formation prescription, and thus it is imperative to use a star formation and feedback prescription that is physically motivated. Until metal-dependent H_2 creation and cooling is added to the simulations, it is not clear how much H I, as opposed to H_2, should be present in the simulation, how it might be distributed as a function of radius, and what impact it will have on the resulting disc.

After applying the physically motivated $\sim 8\,\mathrm{km\,s}^{-1}$ thermal broadening to the Cartesian coordinates of the SPH particles' streaming motion, the inferred *characteristic* velocity dispersions for the cold gas were a reasonable match to those observed in nature (albeit, at the unavoidable expense of recovering any correlation between velocity dispersion and galactocentric radius and/or global star formation in the disc, in addition to the imposition of an isotropic velocity ellipsoid to the cold gas, and the young stars which form from this gas). Beyond the aforementioned issue of the lack of a self-consistent treatment of molecular cooling processings on subparsec scales, one must also be aware that at the resolutions of these simulations, we are still missing unresolved star-forming regions and associated turbulence. The nature of these missing sources is an active area of debate, but magnetorotational instability is one of the favoured mechanisms capable of providing a non-negligible amount of turbulence (e.g. Piontek & Ostriker 2007; Mac Low 2009; Wang & Abel 2009)

Enhancing the SNe energy feedback, as was done for simulation nDG1, at these resolutions, had a marginal impact on the SPH particles' streaming velocities (at the $\sim$20 per cent level), which in turn meant that its impact on the velocity dispersion profiles was also minimal. This is not surprising, as the increased energy deposition was used in order to offset the effect of the newly included high-temperature metal-line cooling. Without the inclusion of extra SN energy, the additional cooling that comes from metal lines leads to more star formation than in the case of DG1. As shown by Oh et al. (2011), the stellar mass of DG1 is in good agreement with galaxies at similar halo masses, as observed by THINGS. If high-temperature metal-line cooling had been added with ϵSN held constant, nDG1 would have overproduced stars for galaxies in a comparable halo mass range. However, the enhanced feedback seems to have steepened the spatial power spectrum of the cold ISM of nDG1 relative to DG1, making it less consistent with the power spectrum observed for the SMC. It is unclear, however, how the power spectrum varies with the instantaneous SFR and if this result holds across time.

Capturing all the relevant ISM physics necessary to recover the full spectrum of turbulence sources at parsec and subparsec scales remains an outstanding challenge. Despite these limitations, the simulated dwarf galaxies presented here have been shown to possess bulk characteristics consistent with those observed in nature, including adherence to scaling relations such as the size–luminosity, size–velocity and luminosity–velocity (Brooks et al. 2011). Additionally, the star formation and feedback prescription used in these simulations has been shown to result in a realistic mass–metallicity relationship as a function of time, and consume gas at a rate that reproduces the incidence rate and metallicities of both quasi-stellar object damped Lyman α (QSO-DLA) and gamma-ray burst DLA systems (Brooks et al. 2007; Pontzen et al. 2008; Pontzen & Pettini 2009).

Hence, it is clear that our simulations remain extremely successful in recovering many of the *global* optical and dynamical properties of realistic bulgeless dwarfs. That is, although the microphysics of the ISM cannot be fully captured at the force resolutions that must be used currently in cosmological simulations, this does not largely impact the bulk macrophysics such as the rotation curves (stellar and dark matter mass profiles), angular momentum content, etc. On the other hand, we have seen that higher resolutions and adoption of more realistic physics for star formation leads to simulated galaxies that better reproduce the properties of observed galaxies (e.g. Booth, Theuns & Okamoto 2007; Robertson & Kravtsov 2008; Saitoh et al. 2008; Tasker & Bryan 2008; Ceverino & Klypin 2009; Governato et al. 2010). The work presented here highlights paths for future improvement in the implementation of ISM physics in cosmological simulations, and provides useful tests for reassessment once metal-dependent H_2 cooling and star formation has been added to GASOLINE and other cosmological simulation codes.

ACKNOWLEDGMENTS

We wish to thank the THINGS team for their insights and access to their exceptional data set, in addition to a number of helpful discussions with F. Governato, A. Pontzen, D. Kawata and A. Burkert and comments from the referee which led to a vastly improved manuscript. BKG and CBB acknowledge the support of the UK's Science & Technology Facilities Council (ST/F002432/1). KP

[9] In large part, this was motivated by the fact that in 'column density space', these high-density regions possess column densities close to $10^{22}\,\mathrm{cm}^{-2}$, higher than those observed in nature; this is a limitation of the conversion employed within GASOLINE.

acknowledges the support of STFC through its PhD Studentship programme (ST/F007701/1). RJT acknowledges support from NSERC, CFI, the CRC program and NSRIT. KP and BKG acknowledge visitor support from Saint Mary's University. We thank the DEISA consortium, cofunded through EU FP6 project RI-031513 and the FP7 project RI-222919, for support within the DEISA Extreme Computing Initative, and the UK's National Cosmology Supercomputer (COSMOS), NASA's Advanced Supercomputing Division, TeraGrid, the Arctic Region Supercomputing Center, and the University of Central Lancashire's High Performance Computing Facility.

REFERENCES

Abadi M. G., Navarro J. F., Steinmetz M., Eke V. R., 2003, ApJ, 591, 499
Bailin J. et al., 2005, ApJ, 627, L17
Bigiel F., Leroy A., Walter F., Blitz L., Brinks E., de Blok W. J. G., Madore B., 2010, AJ, 140, 1213
Bigiel F., Leroy A., Walter F., Brinks E., de Blok W. J. G., Madore B., Thornley M. D., 2008, AJ, 136, 2846
Blanton M. R., Geha M., West A. A., 2008, ApJ, 682, 861
Booth C. M., Theuns T., Okamoto T., 2007, MNRAS, 376, 1588
Brooks A. M., Governato F., Booth C. M., Willman B., Gardner J. P., Wadsley J., Stinson G., Quinn T., 2007, ApJ, 655, L17
Brooks A. M. et al., 2011, ApJ, 728, 51
Ceverino D., Klypin A., 2009, ApJ, 695, 292
Crosthwaite L. P., Turner J. L., Ho P. T. P., 2000, AJ, 119, 1720
Crosthwaite L. P., Turner J. L., Hurt R. L., Levine D. A., Martin R. N., Ho P. T. P., 2001, AJ, 122, 797
Dib S., Bell E., Burkert A., 2006, ApJ, 638, 797
Governato F. et al., 2010, Nat, 463, 203
Governato F. et al., 2004, ApJ, 607, 688
Governato F., Willman B., Mayer L., Brooks A., Stinson G., Valenzuela O., Wadsley J., Quinn T., 2007, MNRAS, 374, 1479
Mac Low M., 2009, Rev. Mex. Astron. Astrofís., Conf. Ser., 27, 121
Monaghan J. J., 1992, ARA&A, 30, 543
O'Brien J. C., Freeman K. C., van der Kruit P. C., 2010, A&A, 515, A62
Oey M. S., Clarke C. J., 1997, MNRAS, 289, 570
Oh S., Brook C., Governato F., Brinks E., Mayer L., de Blok W. J. G., Brooks A., Walter F., 2011, AJ, 142, 24
Okamoto T., Eke V. R., Frenk C. S., Jenkins A., 2005, MNRAS, 363, 1299
Petric A. O., Rupen M. P., 2007, AJ, 134, 1952
Piontek R. A., Ostriker E. C., 2007, ApJ, 663, 183
Pohlen M., Trujillo I., 2006, A&A, 454, 759
Pontzen A. et al., 2008, MNRAS, 390, 1349
Pontzen A., Pettini M., 2009, MNRAS, 393, 557
Robertson B., Yoshida N., Springel V., Hernquist L., 2004, ApJ, 606, 32
Robertson B. E., Kravtsov A. V., 2008, ApJ, 680, 1083
Saitoh T. R., Daisaka H., Kokubo E., Makino J., Okamoto T., Tomisaka K., Wada K., Yoshida N., 2008, PASJ, 60, 667
Sánchez-Blázquez P., Courty S., Gibson B. K., Brook C. B., 2009, MNRAS, 398, 591
Shen S., Wadsley J., Stinson G., 2010, MNRAS, 407, 1581
Sommer-Larsen J., Toft S., Rasmussen J., Pedersen K., Götz M., Portinari L., 2003, Ap&SS, 284, 693
Stanimirovic S., Staveley-Smith L., Dickey J. M., Sault R. J., Snowden S. L., 1999, MNRAS, 302, 417
Stinson G., Seth A., Katz N., Wadsley J., Governato F., Quinn T., 2006, MNRAS, 373, 1074
Stinson G. S., Bailin J., Couchman H., Wadsley J., Shen S., Nickerson S., Brook C., Quinn T., 2010, MNRAS, 408, 812
Stinson G. S., Dalcanton J. J., Quinn T., Gogarten S. M., Kaufmann T., Wadsley J., 2009, MNRAS, 395, 1455
Tamburro D., Rix H., Leroy A. K., Mac Low M., Walter F., Kennicutt R. C., Brinks E., de Blok W. J. G., 2009, AJ, 137, 4424
Tasker E. J., Bryan G. L., 2008, ApJ, 673, 810
Thacker R. J., Couchman H. M. P., 2001, ApJ, 555, L17
van den Bosch F. C., 2001, MNRAS, 327, 1334
van den Bosch F. C., Abel T., Croft R. A. C., Hernquist L., White S. D. M., 2002, ApJ, 576, 21
Wadsley J. W., Stadel J., Quinn T., 2004, New Astron., 9, 137
Walter F., Brinks E., de Blok W. J. G., Bigiel F., Kennicutt R. C., Thornley M. D., Leroy A., 2008, AJ, 136, 2563
Wang P., Abel T., 2009, ApJ, 696, 96

This paper has been typeset from a TEX/LATEX file prepared by the author.